COMPUTER-AIDED DESIGN & APPLICATIONS, 2017
VOL. 14, NO. 6, 815–822
https://doi.org/10.1080/16864360.2017.1287756

Check for updates

Characterization and optimization of an electro-thermal microactuator for precise track positioning

Fan Yang[a], Qikai Xie[b], Xiaolong Zhang [b] and Xiaolin Chen [b]

[a]CGG Americas Inc., USA; [b]Washington State University Vancouver, USA

ABSTRACT

This paper presents a MEMS mirror actuated by four suspended electro-thermal bimorphs. The dimension of the mirror platform is 250 μm × 250 μm. The MEMS mirror design is created based on process modeling following strict fabrication constraints. Transient and dynamic characteristics of the micromirror device are analyzed using coupled electro-thermal-mechanical finite element models and schematic behavior models, respectively. The design is optimized using experimental design and response surface methodology to achieve large actuation displacement and small lateral shift. The micromirror device is shown to have a uniform mirror platform deflection, a large resonant frequency adequate to support the high servo bandwidth control, as well as an excellent linear relation between the micromirror deflection and the input electric power. The proposed electro-thermal MEMS mirror is capable of generating a mirror displacement of 8.25 μm under a 3 *V* pulse voltage input, and can potentially be used as a fine-tracking device for high-density data storage applications.

KEYWORDS

Precise positioning; coupled analysis; schematic model; optimization

1. Introduction

Micro-electro-mechanical systems (MEMS)-based mirrors are widely used in applications including optical displays, biomedical imaging, optical interconnects, optical switching, and laser beam steering [4, 8]. In data storage devices for instance, in order to achieve high precision optical tracking, the dual stage tracking scheme is often employed using a voice coil motor as primary stage for coarse positioning and a MEMS mirror actuator as second stage for fine tracking [11]. The miniature MEMS mirror actuator is the key component to provide the driving force for the second stage precise positioning in such devices. Various actuation mechanisms have been proposed to drive the micro mirrors, including electrostatic, electromagnetic, piezoelectric and electro-thermal techniques. Among the studies, electrostatic MEMS mirrors with standard gimbal mount configuration, tripod design, or stacked comb drives have been designed and fabricated. Electrostatically actuated micromirrors typically have good linearity compared to piezo-actuated devices and fast response [10]. However, in such devices, suitable encapsulation is essential so as to offer low driving voltage and protection against contamination by particles. Electromagnetic micromirrors can achieve large deflections under small current inputs, yet the efficiency of the force generated in the electromagnetic field and the high power consumption remain a challenge in electromagnetic micromirrors [6]. Piezoelectric micromirrors have potential merits in tracking speed and power consumption due to the non-contact mechanism, however, they involve complex fabrication steps that are not compatible with standard IC process [1, 11]. Compared to other actuating approaches, electro-thermal micromirrors have characteristics of large displacement, large force, low actuating voltage and low power consumption [2, 7, 9]. Besides, their device fabrication process is relatively simple and fully compatible with the general integrated circuit (IC) fabrication process.

In this paper, we present an electro-thermal bimorph-based micromirror actuated by folded beam suspensions. The micromirror actuator has four folded bimorph beams, which are linked to the micromirror platform at four corners via linkage hinges. Due to the bimorph effect, the folded-beams deform under the actuating voltage and move the integrated micromirror platform along its surface normal direction. Such a micromirror actuator can be mounted inside the optical pickup head to alter the path of the laser beams for precise track positioning. The paper is organized as follows: Section 2 describes the design model creation for the device by

CONTACT Fan Yang fanyang.nick@gmail.com; Qikai Xie qikai.xie@wsu.edu; Xiaolong Zhang xiaolong.zhang@wsu.edu; Xiaolin Chen chenx@wsu.edu

© 2017 CAD Solutions, LLC, http://www.cadanda.com

integrating mask layouts and the associated fabrication process sequence. The coupled physics of the device is modeled with detailed finite element simulations solving a coupled set of physical constitutive equations in several energy domains. Section 3 presents the coupled finite element analysis for evaluating the device transient characteristics. Section 4 presents a schematic behavior model for the device frequency domain characterization. Design of experiments and response surface optimization are then utilized to determine the optimal parameter settings for the device under given constraints and specifications, with results presented in section 5. Section 6 gives the conclusion.

2. Design and fabrication process modeling

We create the microactuator design using CoventorWare by taking the device manufacturability into consideration. A 3-D design geometry is developed by the deposition and etching of different layers of materials based on parameterized layout designs and standard photolithography steps. Fig. 1(a) shows the design layout, in which a 200μm × 200 μm micromirror is deposited on top of a 250μm × 250 μm substrate platform at the center and connected to four folded beams through two L-shaped metal heaters. Each folded beam is made of two identical arms. Each arm consists of a 125 μm long silicon-dioxide-on-silicon bimorph section and a 115 μm long aluminum-on-silicon bimorph section. Fig. 1(b) illustrates the folded beam configuration. The identical arm design ensures that the mirror remains planar after deformation, as the folded-beam suspension which is fixed at *A* is able to achieve a zero rotation at the lifted end *B* (see Fig. 1(b)).

Fig. 2 illustrates the critical process modeling steps. As shown in Fig. 2, a 2 μm thick thermal oxide layer is deposited on the silicon wafer substrate as the sacrificial layer. The entire device is then covered by a 2 μm thick doping silicon layer and then a 1.5 μm thick silicon dioxide layer. Next, silicon dioxide and aluminum are patterned through photolithography to create the top layer of bimorph sections, respectively. Back side etching of silicon substrate is then performed, and the doping silicon layer of the bimorph beams is constructed by etching through the thermal oxide layer from the top side. Then, a thin film of gold is sputtered on the device surface to form the micromirror and heaters. The final step is to strip off the sacrificial layer to release the suspension structure. Tab. 1 summarizes the key fabrication steps, material selections and the corresponding film thicknesses. Properties of the silicon-based materials used in the bimorph are given in Tab. 2.

3. Coupled electro-thermal-mechanical analysis

The device design, developed based on mask set and process sequence, is analyzed to investigate its thermal and mechanical behaviors. Coupled electro-thermal-mechanical simulation is performed to determine the voltage, current density, temperature and deformation distributions of the micromirror actuator under a small voltage input. The boundary and initial conditions are given as follows: the folded beams are fixed at the four protruding ends, and the four fixed ends are assumed to be at a 20°C room temperature. A 3 *V* pulse voltage input with a 2 *ms* pulse period composed of a 500μs on time and a 1500μs off time, as shown in Fig. 3, is applied to two opposite ends of the folded beams, with the other

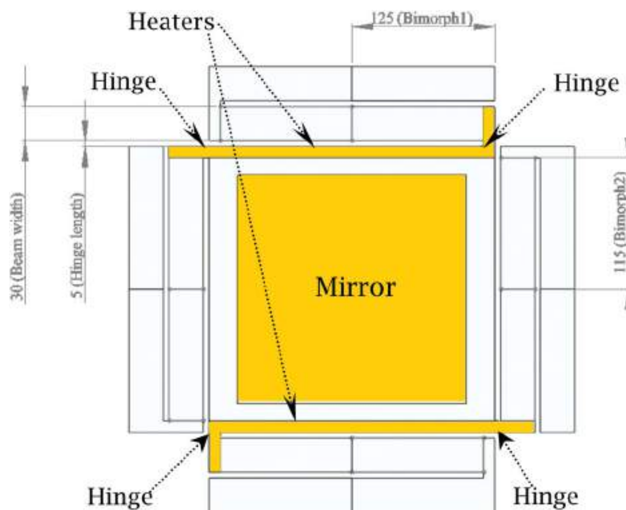

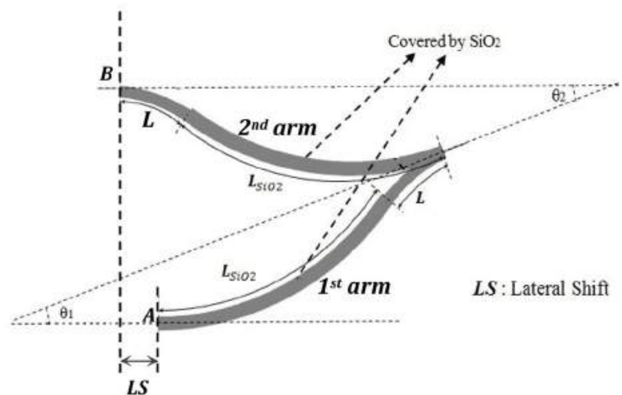

Figure 1. Fabrication process based design modeling with figures from left to right: (a) 2D layout of the folded-beam microactuator (Unit: μm), (b) The folded-beam configuration.

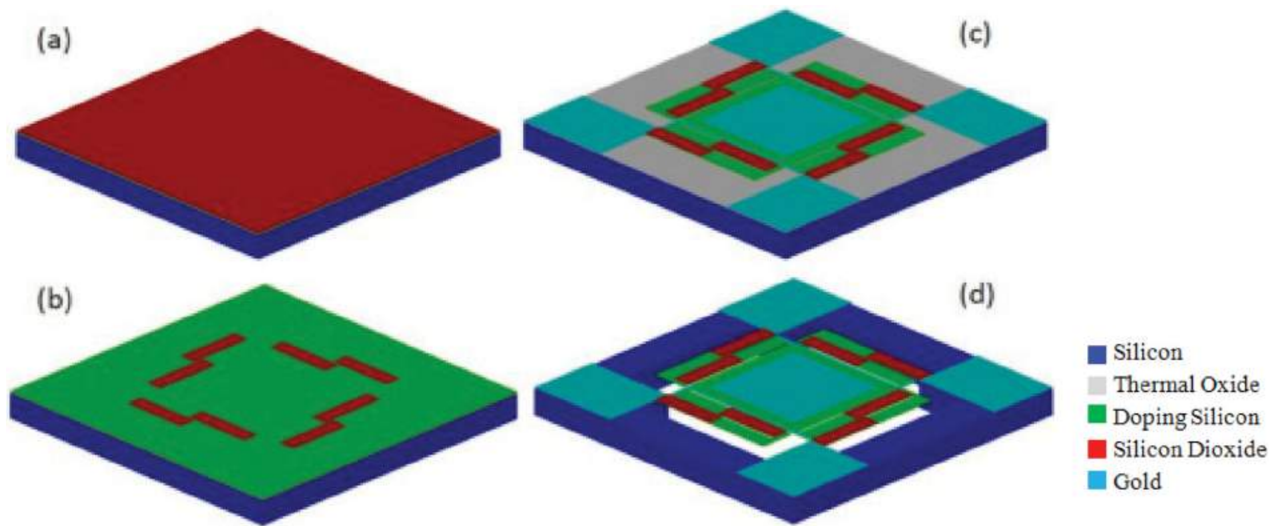

Figure 2. Deposition and etching of different material layers.

Table 1. Key fabrication steps of the microactuator.

	Step Name	Material	Thickness
1	Substrate	Silicon	50 µm
2	Sacrificial layer deposition	Thermal oxide	2µm
3	Bimorph bottom layer deposition	Doping silicon	2µm
4	Bimorph top layer deposition	Silicon dioxide	1.5µm
5	Bimorph top layer patterning	Silicon dioxide/ Aluminum	15 µm/0.1 µm
6	Substrate patterning	Silicon	50µm
7	Bimorph bottom layer patterning	Doping silicon	2µm
8	Mirror sputtering	Gold	0.1µm
9	Heater sputtering	Gold	1.0µm
10	Sacrificial layer removal	Thermal oxide	2µm

Table 2. Properties of silicon-based materials used in the bimorph.

Materials	Doping Si	Si dioxide
Young's modulus (MPa)	1.6×10^5	0.70×10^5
Poisson ratio	0.17	0.17
Density (kg·µm^{-3})	2.42×10^{-15}	2.66×10^{-15}
Specific heat (pJ·kg^{-1}·K^{-1})	7.12×10^{14}	10.00×10^{14}
Resistivity (TΩ·µm)	3.46×10^{-11}	1.00×10^{10}
Coefficient of thermal expansion (K^{-1})	2.60×10^{-6}	0.50×10^{-6}
Thermal conductivity (pW·µm^{-1}·K^{-1})	1.48×10^8	1.04×10^6

two ends left grounded. The initial temperature of the whole structure is set up as the room temperature of 20°*C*. Fig. 4 gives the derived results from the coupled analysis. As expected, the current density maintains a relatively high value along the two L-shaped metal heaters. The maximum temperature occurs along the second arm of the folded-beam. The induced mirror deflection is fairly uniform. The entire mirror platform is found to be lifted up 1.6µm by the folded-beams under a 3 *V* pulse voltage input.

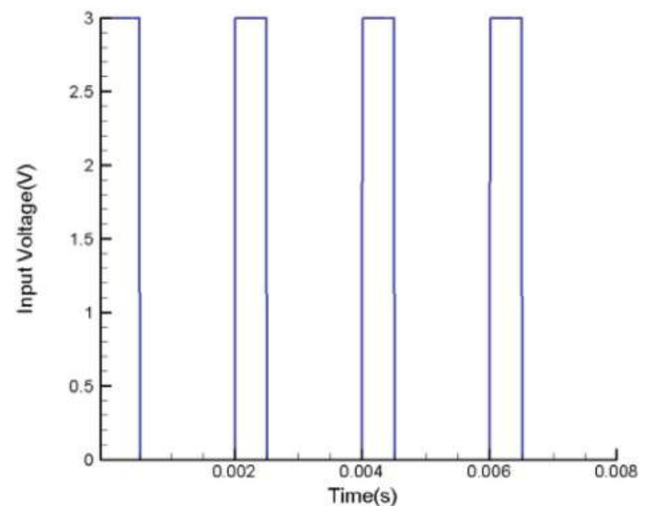

Figure 3. Heating pulse voltage input (4 cycles): 3 *V* amplitude, 500µs pulse on and 1500µs pulse off time.

An excellent linear relation of the electro-thermally induced mirror deflection and the input electric power is also observed from the design model investigation, as shown in Fig. 5.

4. Frequency response characterization

For frequency-domain characterization of the electro-thermal microactuator, behavioral modeling is conducted as frequency response analysis is overwhelming for the finite element approach due to the many thin material layers involved. A behavior model is assembled for the design by inserting parameterized components

Figure 4. Coupled finite element simulation results with figures: (a) Voltage distribution (unit: V), (b) Current density distribution (unit: pA/ μm^2), (c) Temperature distribution (unit: K), (d) Z-displacement distribution (unit: μm).

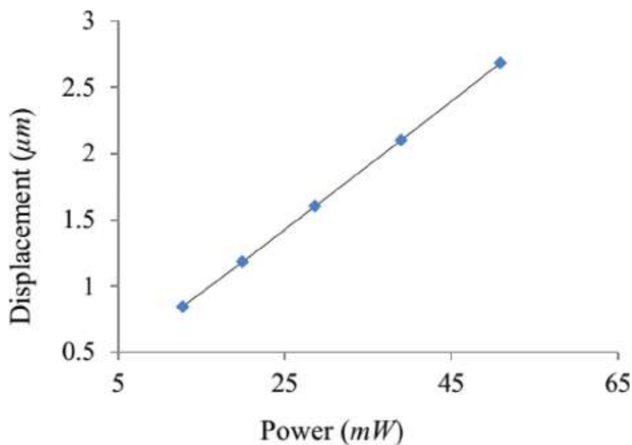

Figure 5. Mirror deflection versus input power.

from the MEMS Component Library in CoventorWare. Parametric information about a component such as material property, layer thickness and geometry dimensions are included as component parameters in the behavioral model. Fig. 6 shows the schematic behavior model developed for the microactuator.

The device's behavioral model is taken for frequency analysis and its frequency response is presented in Fig. 7, which shows that the fundamental resonant frequency of the device is estimated to be 17.8*kHz*, successfully meeting the high servo bandwidth control frequency requirement of over 10*kHz*.

A design sensitivity analysis is next conducted to investigate the effects of geometric perturbation on the device's frequency and mirror deflection performance. Tab. 3 shows the sensitivity to parameter variations in the design, assuming a 10% design parameter perturbation. Four design parameters are investigated, namely, the overall beam length, beam width, hinge length and hinge width (See Figs. 1 and 6). The analysis reveals that the resonant frequency and the mirror deflection are most sensitive to the beam length change. A 10% variation in beam length will lead to a resonant frequency drift of 696 *Hz* and a mirror displacement drift of 0.311 μm, compared

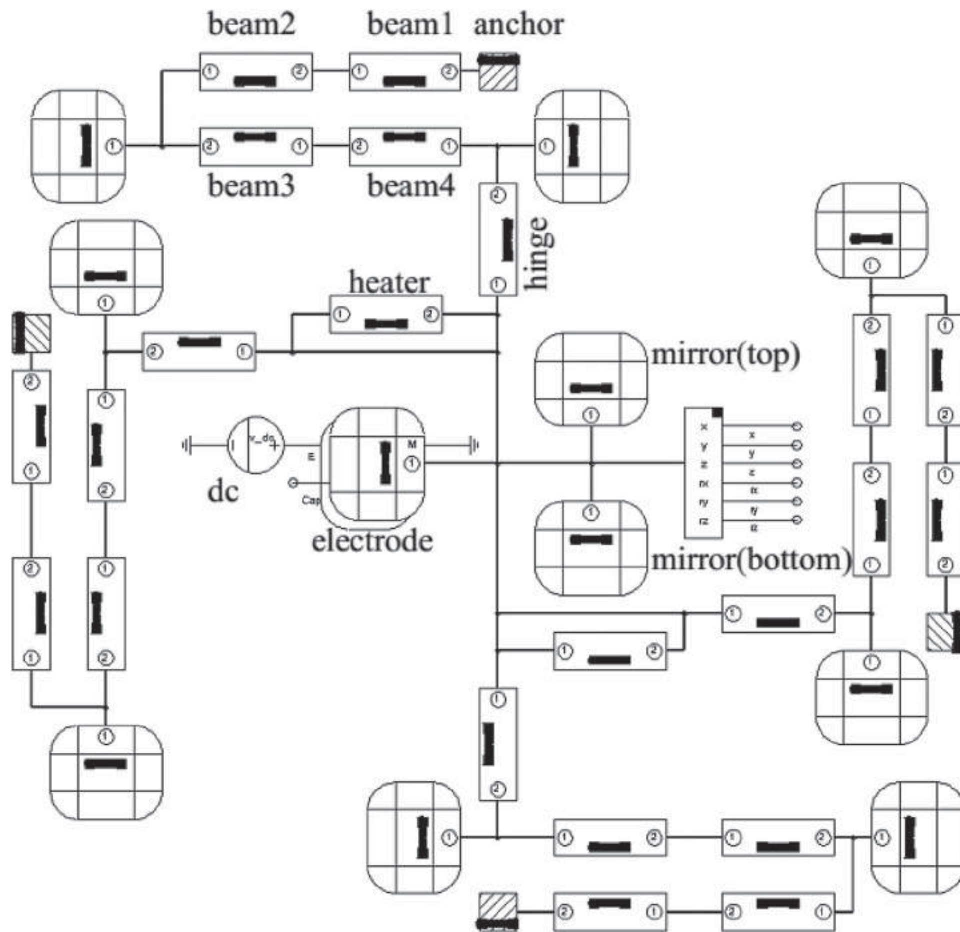

Figure 6. Behavioral model of the microactuator.

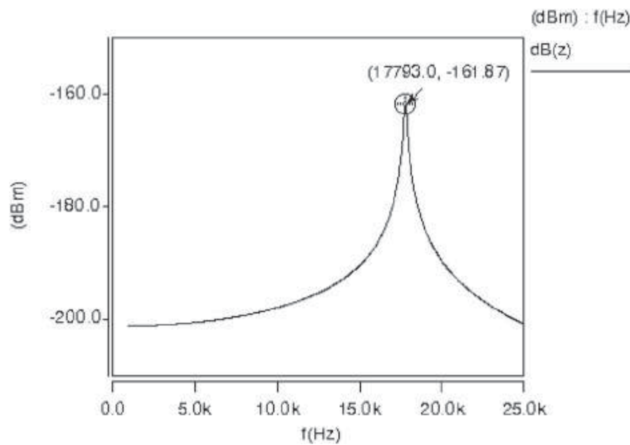

Figure 7. Frequency response of the microactuator.

to a frequency drift of 279 *Hz* and a displacement drift of 0.0086 μm due to 10% variation in beam width.

5. Response surface optimization

To evaluate trade-offs and generate an optimal design, response surface modeling (RSM) [3, 5] and design of experiments (DOE) are next carried out for the multi-parameter optimization task. Through careful design of experiments, a polynomial model, also called response surface model, is built and utilized to predict the relationship between the response characteristics and the design parameters. To predict better solution candidates, we employ sequential quadratic programming (SQP) algorithm on the response surface models. The optimization process is illustrated in the flowchart in Fig. 8.

The response parameters of greatest concern for the microactuator design are identified as follows: the mirror deflection and the mirror lateral shift. Two independent

Table 3. The effects of design parameter variation (10% perturbation).

	beam		hinge	
	length	width	length	width
Nominal size (μm)	250	30	5	10
Geometric perturbation (μm)	25	3.0	0.5	1.0
Frequency shift (*Hz*)	696	279	62.3	109
Sensitivity (frequency)	0.391	0.157	0.035	0.061
Displacement shift (*nm*)	311	8.6	6.5	2.9
Sensitivity (displacement)	1.85	0.053	0.040	0.018

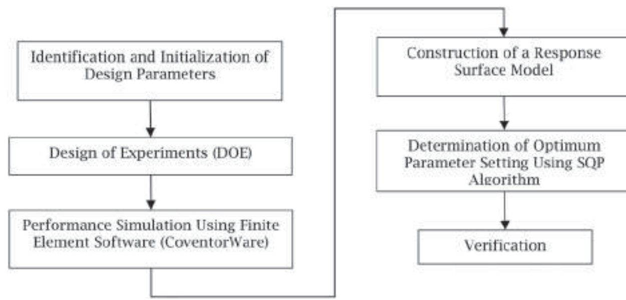

Figure 8. Flow chart of the response surface based optimization process.

variables are chosen as the design parameters, namely, the length (L) of the aluminum-on-silicon bimorph section and thickness (T) of the aluminum layer, due to their high sensitivities to the response parameters. The constraints for the design parameters are set as: $20\mu m \leq L \leq 80\mu m$ and $0.08\mu m \leq T \leq 0.22\mu m$.

We employ the central composite design (CCD) in our design of experiment plan. The design space is sampled through the CCD, with the response dataset obtained for each design scenario through the coupled finite element simulation in CoventorWare. The study levels of the CCD and corresponding values of design parameters are listed in Tab. 4. Tab. 5 gives the responses (the mirror deflection and the lateral shift) for each combination of the design parameter.

We adopt a quadratic response surface model in the form given in Eqn. (1):

$$Y = b_0 + \sum_i b_i x_i + \sum_i b_{ii} x_i^2 + \sum_{i<j} b_{ij} x_i x_j + \varepsilon \quad (1)$$

where Y stands for the response; x_i is the ith controlled variable (design parameter), b_i, b_{ij} are the ith and ij^{th} estimated regression coefficient, respectively. ϵ is the error.

Table 4. Design parameter values of different levels for the optimization study.

Level	−1.414	−1	0	1	1.414
L (μm)	21.72	30	50	70	78.28
T (μm)	0.08	0.10	0.15	0.20	0.22

Table 5. Experimental Design and simulation results of the responses.

No.	L	T	Deflection (μm)	Lateral Shift (μm)
1	−1	−1	2.5536	−0.0015
2	1	−1	5.4213	0.0244
3	−1	1	4.2691	0.0081
4	1	1	8.7138	0.1012
5	−1.414	0	2.5140	−0.0012
6	1.414	0	7.7413	0.0774
7	0	−1.414	3.5370	0.0024
8	0	1.141	7.1867	0.0533
9	0	0	5.4891	0.0230

With a set of experimental results from the CCD, Eqn. (1) can be rewritten using matrix notation:

$$\mathbf{Y} = \mathbf{XB} + \varepsilon \quad (2)$$

where $\mathbf{Y}$ is a vector of response characteristic obtained from the CCD; $\mathbf{X}$ is the matrix containing the values of the design variables; $\mathbf{B}$ is the vector of regression coefficient and ε is a vector of errors. They are given as:

$$\mathbf{X} = \begin{bmatrix} 1 & x_{11}\cdots x_{1k} & x_{11}^2\cdots x_{1k}^2 & x_{11}x_{12}\cdots x_{1(k-1)}x_{1k} \\ 1 & x_{21}\cdots x_{2k} & x_{21}^2\cdots x_{2k}^2 & x_{21}x_{22}\cdots x_{2(k-1)}x_{2k} \\ \vdots & \vdots & \vdots & \vdots \\ 1 & x_{k1}\cdots x_{kk} & x_{k1}^2\cdots x_{kk}^2 & x_{k1}x_{k2}\cdots x_{k(k-1)}x_{kk} \end{bmatrix}$$

$$\mathbf{Y} = \begin{bmatrix} Y_1 \\ Y_2 \\ \vdots \\ Y_k \end{bmatrix}$$

$$\mathbf{B} = \begin{bmatrix} b_0 \\ b_1 \\ \vdots \\ b_k \end{bmatrix}, \boldsymbol{\varepsilon} = \begin{bmatrix} \varepsilon_1 \\ \varepsilon_2 \\ \vdots \\ \varepsilon_\kappa \end{bmatrix}$$

where k is the number of experiments.

By applying least squares method, the estimate $\tilde{\mathbf{B}}$ of the coefficient $\mathbf{B}$ can be obtained as follows:

$$\tilde{B} = (\mathbf{X}^T\mathbf{X})^{-1}\mathbf{X}^T\mathbf{Y} \quad (3)$$

Finally, the fitted second-order response surface model is given as:

$$\tilde{\mathbf{Y}} = \mathbf{X}\tilde{\mathbf{B}} \quad (4)$$

The optimal set of controlled variables, with which the value of $\tilde{\mathbf{Y}}$ is maximized (or minimized), can then be determined by applying sequential quadratic programming (SQP) optimization algorithm which is integrated in the open-source OPTI Toolbox, a MATLAB Toolbox for Optimization.

Using the above-mentioned RSM procedure, the response surface models for the mirror deflection (D) and mirror lateral shift (LS) can be obtained as follows based on data presented in Tabs. 4 and 5:

$$D = 5.4891 + 1.8383L + 1.2713T - 0.1821L^2 - 0.0650T^2 + 0.3943L \times T \quad (5)$$

$$LS = 0.0230 + 0.0288L + 0.0198T + 0.0076L^2 + 0.0025T^2 + 0.0168L \times T \quad (6)$$

The design objective is set so as to maximize the mirror deflection (D) under a lateral shift (LS) of no greater

than 1% of the mirror deflection, i.e., $LS \leq 0.01D$. The optimal parameter settings are determined by applying the SQP optimization algorithm. Fig. 9 shows the infeasible and feasible design regions. The line with hash marks represents where LS equals to 1% of D. The optimal point is found to be at the location with coordinates of (0.5016, 1.3700) in the design space, which correspond to $L = 60.03\mu m$ and $T = 0.22\mu m$. The optimal mirror deflection and the lateral shift can thus be found by Eqns. (5) and (6) as 8.25μm and 0.0825μm, respectively.

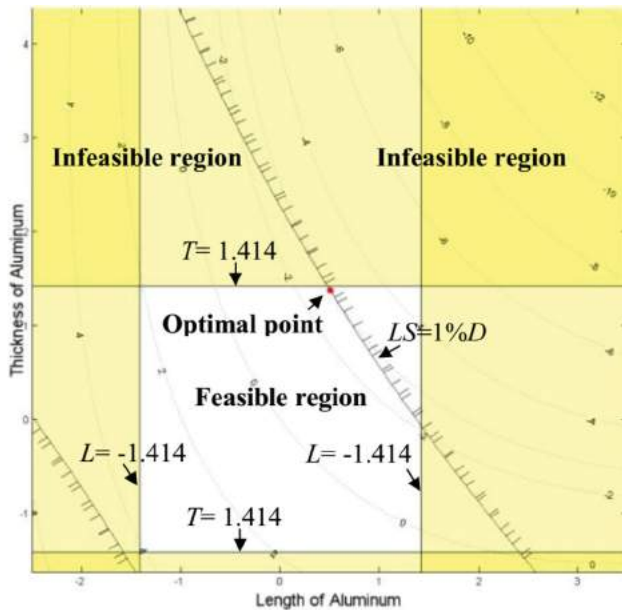

Figure 9. Contour of the design response surface model.

Fig. 10 shows the deformation of the optimum design. As shown, a fairly large vertical displacement of about 8.25μm is generated in the mirror platform, with only a negligibly small amount of lateral shift introduced.

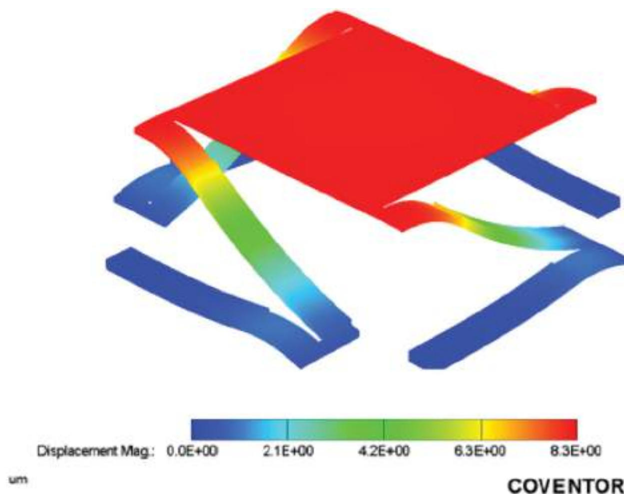

Figure 10. Deformation plot of the optimum design.

The frequency response presented in Fig. 11 shows that the fundamental resonant frequency of the optimized design is around 14.8kHz, which also meets the design criteria of having a high bandwidth of over 10kHz for servo control.

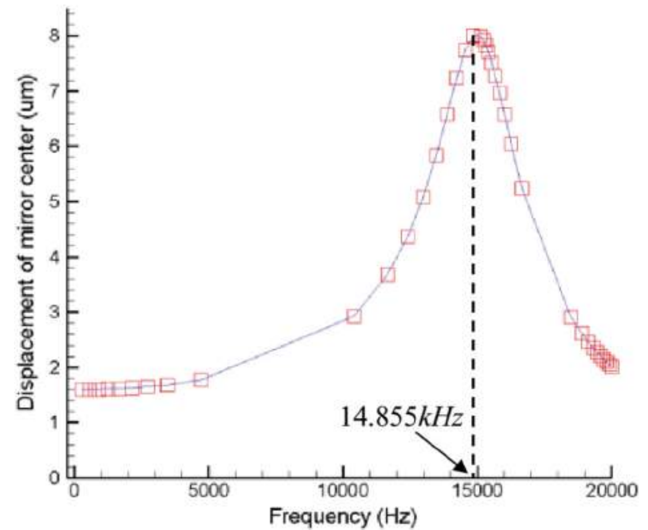

Figure 11. Frequency response of the optimized microactuator.

6. Conclusions

In this work, design characterization and optimization is conducted on an electro-thermal bimorph-based microactuator. Coupled electro-thermal-mechanical simulation is carried out to investigate the voltage, current density, and induced temperature and deformation distributions as well as the effects of dimensional variations on device performance. The frequency domain behaviors are characterized using a schematic behavior model. To obtain an optimal response, a second-degree response surface model is used to attain specified design goals. Our results show that the optimal design is capable of generating a large mirror deflection of 8.25 μm, while maintaining mirror flatness and introducing only a negligible lateral shift of 0.0825 μm. The resonant frequency of the optimized design is estimated to be around 14.8 kHz, which is adequate to support high servo bandwidth control. The microactuator also achieves an excellent linear relation between mirror deflection and input power, and can potentially be used as an effective fine-tracking device for high-density data storage applications.

Acknowledgements

We would like to express our sincere thanks to Dr. Jiaping Yang at A*STAR Data Storage Institute in Singapore for the helpful discussions he provided about the work.

ORCID

Xiaolong Zhang http://orcid.org/0000-0003-0657-7786

Xiaolin Chen http://orcid.org/0000-0002-8760-6480

References

[1] Chao, P. C.-P.; Liao, L.-D.; Lin, H.-H.;Chung, M.-H.: Robust dual-stage and repetitive control designs for an optical pickup with parallel cantilever beams powered by piezo-actuation, Microsystem Technologies, 16(1), 2009, 317–331. doi:10.1007/s00542-009-0909-z

[2] Chen, W.-C.; Chu, C.-C.; Hsieh, J.; Fang, W.: A reliable single-layer out-of-plane micromachined thermal actuator, Sensors and Actuators A: Physical, 103(1–2), 2003, 48–58. doi:10.1016/S0924-4247(02)00315-1

[3] Chen, S.; Yang, J.; Mou, J.;Lu, Y.: Quality based design approach for a single crystal silicon microactuator using DOE technique and response surface model, Microsystem technologies, 8(2–3), 2002, 182–187. doi:10.1007/S00542-001-0128-8

[4] Cheng, S.; Chou, P.: Adaptive ZPETC method for dual-stage actuator controller design in miniaturized optical disc drive, Proc. 2008 IEEE 14th International Mixed-Signals, Sensors, and Systems Test Workshop, 1–6. doi:10.1109/IMS3TW.2008. 4581603

[5] Khuri, A. I.; Mukhopadhyay, S.: Response surface methodology, Wiley Interdisciplinary Reviews: Computational Statistics, 2(2), 2010, 128–149. doi:10.1002/wics.73

[6] Ko, J. S.; Lee, M. L.; Lee, D.-S.; Choi, C. A.;Tae Kim, Y.: Development and application of a laterally driven electromagnetic microactuator, Applied Physics Letters, 81(3), 2002, 547–549. http://dx.doi.org/10.1063/1.1494462

[7] Tsai, C.-H.; Tsai, C.-W.; Chang, H.-T.; Liu, S.-H.;Tsai, J.-C.: Electrothermally-Actuated Micromirrors with Bimorph Actuators—Bending-Type and Torsion-Type, Sensors, 15(6), 2015, 14745–14756. http://dx.doi.org/10.3390/s150614745

[8] Watanabe, I.; Ikai, Y.; Kawabe, T.; Kobayashi, H.; Ueda, S.; Ichihara, J.: Precise track-following control using a MEMS tracking mirror in high-density optical disk drives, Proc. 2002 International Symposium on Optical Memory and Optical Data Storage Topical Meeting, 2002, 257–259. http://dx.doi.org/10.1109/OMODS.2002.1028633

[9] Yang, J.; Deng, X.;Chong, T.: An electro-thermal bimorph-based microactuator for precise track-positioning of optical disk drives, Journal of Micromechanics and Microengineering, 15(5), 2005, 958–965. http://dx.doi.org/10.1088/0960-1317/15/5/009

[10] Yang, J. P.; Low, L. N.; Johnson, D.: A MEMS-based tracking milli-mirror for high-density optical disk drives, Sensors and Actuators A: Physical, 133(2), 2007, 368–374. doi: 10.1016/j.sna.2006.06.019

[11] Yee, Y.; Nam, H.-J.; Lee, S.-H.; Bu, J. U.; Lee, J.-W.: PZT actuated micromirror for fine-tracking mechanism of high-density optical data storage, Sensors and Actuators A: Physical, 89(1–2), 2001, 166–173. doi:10.1016/S0924-4247(00)00535-5